Equilibrium shapes of tubular lipid membranes, Supplementary Information

U. Jelerčič
Jožef Stefan Institute, Jamova 39, SI-1000 Ljubljana, Slovenia

ANALYTICAL APPROXIMATIONS

Branches A1 and A2

The structure of the helical shape in branch A2 is modelled as a tube wrapped around a helix and can be parameterised as:

$$\begin{aligned} x &= \cos t\,(R + r_c \cos\theta) + \frac{c r_c \sin t \sin\theta}{\sqrt{c^2+R^2}}, \\ y &= \sin t\,(R + r_c \cos\theta) - \frac{c r_c \cos t \sin\theta}{\sqrt{c^2+R^2}}, \\ z &= ct + \frac{R r_c \sin\theta}{\sqrt{c^2+R^2}}. \end{aligned} \tag{1}$$

Here θ denotes the angle of the tube [$\theta \in (0, 2\pi)$] and $t \in (0, 2\pi)$. R and r_c correspond to the radius of the helix and the radius of the tube, respectively, and $2\pi c$ is the helix pitch (Fig. 1).

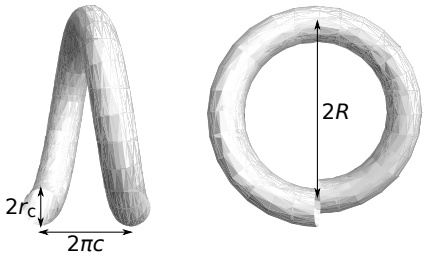

FIG. 1. **Analytical model used for the helical branch A2.** R and r_c correspond to the helix and tube radius, respectively and $2\pi c$ is helix pitch (left: lengthwise view, right: axial view).

The volume, surface area, segment length and bending energy can be then expressed as

$$V = 2\pi^2 r_c^2 \sqrt{c^2+R^2}, \tag{2}$$

$$A = 4\pi^2 r_c \sqrt{c^2+R^2}, \tag{3}$$

$$L = 2\pi c, \tag{4}$$

$$F = 8\pi\kappa \frac{\pi\left(c^2+R^2\right)^{3/2}}{4r_c\sqrt{\left(c^2+R^2\right)^2 - R^2 r_c^2}}. \tag{5}$$

We model the snake-like structure in branch A1 by using an undulated backbone with a tube wrapped around it (Fig. 2a). The backbone is assumed to be sinusoidal at segment lengths close to L_{cyl} and the parameterisation is:

$$\begin{aligned} x &= r_c \sin\theta, \\ y &= R\sin t \mp \frac{c r_c \cos\theta}{\sqrt{c^2 + R^2\cos^2 t}}, \\ z &= ct \pm \frac{R r_c \cos t \cos\theta}{\sqrt{c^2+R^2\cos^2 t}}, \end{aligned} \tag{6}$$

where the top and bottom signs correspond to $t \in (0, \pi)$ and $t \in (\pi, 2\pi)$, respectively. The volume, surface area, segment length, and bending energy are too tedious to be spelled out.

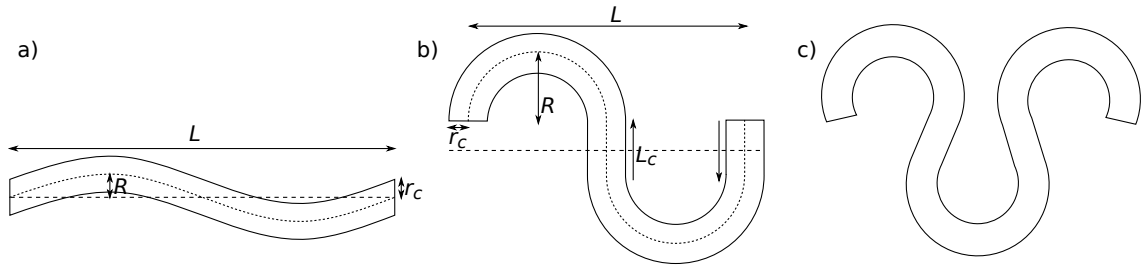

FIG. 2. **Analytical models used for the snake-like branch A1.** a) Sinusoidal model relevant for segment lengths close to L_{cyl}. b) Toroidal model used to describe the rest of the branch. c) Schematic representation of a possible snake-like shape at extremely small segment lengths. This regime is not covered in our analytical analysis.

As the segment length is decreased, the tubular shape is compressed and the sinusoidal ansatz is no longer adequate. In this case we take into account shape which is comprised of two toroidal halves connected by a straight cylindrical part (Fig. 2b). The geometric constraints and the corresponding bending energy are

$$V = 2\pi^2 R r_c^2 + L_c \pi r_c^2, \tag{7}$$

$$A = 4\pi^2 R r_c + 2L_c \pi r_c, \tag{8}$$

$$L = 4R, \tag{9}$$

$$F = \frac{8\pi^2 \kappa R^2}{4r_c\sqrt{R^2 - r_c^2}} + \pi\kappa \frac{L_c}{r_c}. \tag{10}$$

We note that even this shape does not represent a universally applicable approximation, since the tubular structure is deformed further as L is decreased (Fig. 2c). However, at small reduced volumes relevant in cellular environment, this happens at segment lengths so low that they do not represent the focus of our analysis.

Branch B

The structure in branch B is approximated by a cylindrical segment of radius r_c and length L_c connected to an axisymmetric body. We model the body in three different ways: i) as a sphere, ii) as a spherocylinder, and iii) as an ellipsoid (Fig. 3).

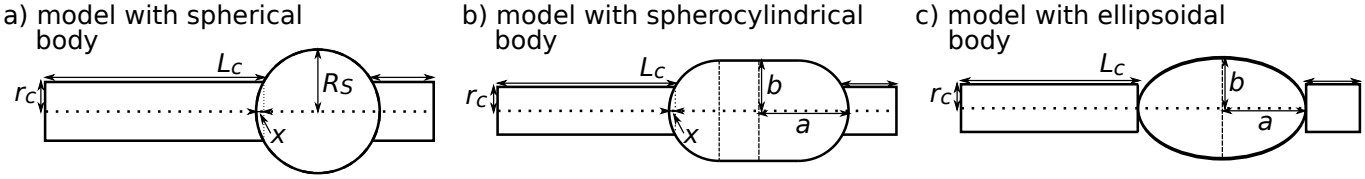

FIG. 3. **Analytical approximations for the tube with an ellipsoidal body in branch B.** a) Model with a spherical body of radius R_s, representing the simplest and the most crude approximation. b) Model with a spherocylindrical body constructed using two hemispheres of radius b and a cylindrical part of length $a - b$ in between. c) The most exact model assuming an axisymmetric ellipsoidal body with semiaxes a and b. In this case, the juncture between the body and the cylindrical portion is less exact.

The volume, surface area, segment length, and free energy for all three models are as follows.
Spherical body model:

$$\begin{aligned} V &= \pi r_c^2 L_c + \frac{4}{3}\pi R_s^3 - \frac{\pi x}{3}\left(3r_c^2 + x^2\right), \\ A &= 2\pi r_c L_c + 4\pi R_s^2 - 4\pi R_s x, \\ L &= L_c + 2R_s - 2x, \\ F &= 8\pi\kappa\left(1 + \frac{1}{8}\frac{L_c}{r_c} - \frac{x}{R_s}\right), \quad x = R_s - \sqrt{R_s^2 - r_c^2}. \end{aligned} \tag{11}$$

Spherocylindrical body model:

$$
\begin{aligned}
V &= \pi r_c^2 L_c + 2\pi b^2(a-b) + \frac{4}{3}\pi b^3 - \frac{\pi x}{3}\left(3r_c^2 + x^2\right), \\
A &= 2\pi r_c L_c + 4\pi b(a-b) + 4\pi b^2 - 4\pi b x, \\
L &= L_c + 2a - 2x, \\
F &= 8\pi\kappa\left(1 + \frac{1}{8}\frac{L_c}{r_c} + \frac{a-b}{4b} - \frac{x}{b}\right), \quad x = b - \sqrt{b^2 - r_c^2}.
\end{aligned} \tag{12}
$$

Ellipsoidal body model:

$$
\begin{aligned}
V &= \pi r_c^2 L_c + \frac{4}{3}ab^2\pi, \\
A &= 2\pi r_c L_c + 2\pi b\left[b + \frac{a^2 \arccos\left(b/a\right)}{\sqrt{a^2 - b^2}}\right], \\
L &= L_c + 2a, \\
F &= 8\pi\kappa\left(\frac{1}{8}\frac{L_c}{r_c} + \right. \\
&\left. \int_0^{\pi}\int_0^{2\pi} \frac{a^2 \sin(v)\left\{3a^2 + (a^2 - b^2)\left[\cos(2v) - 2\cos(2u)\sin^2(v)\right] + 5b^2\right\}^2}{256\pi b\left\{\sin^2(v)\left[a^2\sin^2(u) + b^2\cos^2(u)\right] + a^2\cos^2(v)\right\}^{5/2}} \mathrm{d}u\mathrm{d}v\right).
\end{aligned} \tag{13}
$$

The three models do not differ significantly, especially if we are only interested in the free energy of the structures. Depending on the level of structural detail we wish to determine, an appropriate model is chosen. We note that we used the spherocylindrical body model for the calculations presented in the paper.

Branch C

The simplest possible ansatz that describes the flattened discoidal body in branch C is comprised of a cylindrical part and a torus or a torus section with a flat circular membrane parallel to the tube (Fig. 4).

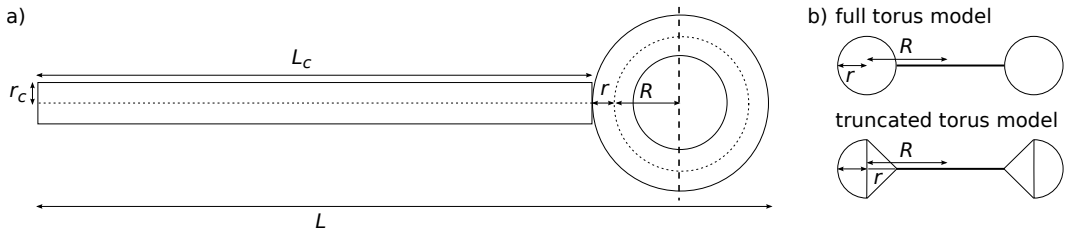

FIG. 4. **Analytical approximation of tube with a discoidal body in branch C.** a) Schematic representation of the whole structure in top view. b) Two variants of the discoidal body cross-section shape, which differ in the way the rim portion is approximated. The cross-sections correspond to the part of the circular structure marked by the vertical dashed line.

In the case of the full torus model, the volume, surface area, segment length, and the bending energy read

$$
\begin{aligned}
V &= \pi r_c^2 L + 2\pi^2 R r^2, \\
A &= 2\pi r_c L + 4\pi^2 R r + 2\pi(R - r)^2, \\
L &= L + 2(R + r), \\
F &= \pi\kappa\frac{L}{r_c} + 2\pi^2\kappa\frac{R^2}{r\sqrt{R^2 - r^2}},
\end{aligned} \tag{14}
$$

respectively, and in the truncated torus model (used for calculations presented in the paper) they are given by

$$
\begin{aligned}
V &= \frac{1}{3}\pi(4r+3\pi R)r^2 + 2\pi R^2 r + L_c\pi r_c^2 - \frac{2}{3}\pi\left[R^3-(R-r)^3\right], \\
A &= 2\pi(R-r)^2 + 2\sqrt{2}\pi r(2R-r) + 2\pi r(2r+\pi R) + 2L_c\pi r_c, \\
L &= L + 2(R+r), \\
F &= 8\pi\kappa\left\{1 + \frac{L_c}{8r_c} + \frac{R^2\left[5\tan^{-1}\left(\sqrt{\frac{R-r}{R+r}}\right) + 4\tan^{-1}\left(\frac{r-R}{\sqrt{R^2-r^2}}\right)\right]}{2r\sqrt{R^2-r^2}}\right\}.
\end{aligned}
\tag{15}
$$

We note that in numerical solutions the assumption of a flat central part is enforced manually due to computational reasons. An alternative to the flat shape is a curved morphology of the discoidal body and since it cannot be easily found using our numerical approach, we explore this possibility analytically (Fig. 5).

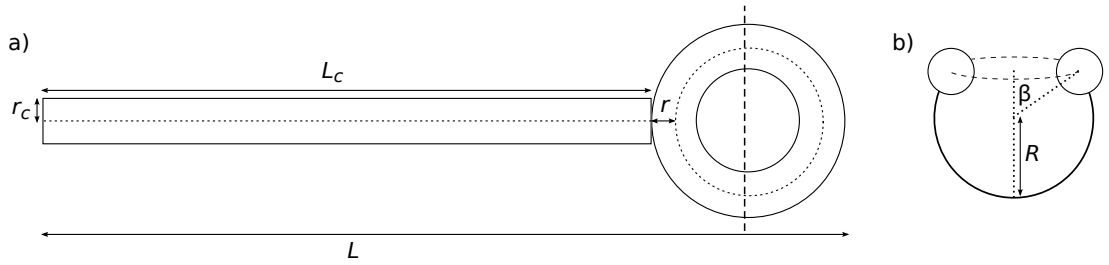

FIG. 5. **Curved shape of discoidal body in branch C.** a) Top view of the whole structure including the tubular and discoidal part and b) cross-section of the reservoir at the position marked by a vertical dashed line. Angle β represents the degree of curvature and is limited to $\beta \in (0, \pi)$.

We find that the curved shape is energetically preferred at small segment lengths, whereas at $L \sim L_{cyl}$ the body is expected to have a flat central part (Fig. 6). This transition is evident if we focus on the angle β used here to qualitatively characterise the overall curvature of the body. The angle increases and diverges as the values of segment length approach L_{cyl}, indicating that the transition between the decreasingly curved and the flat shape is indeed expected. We point out, however, that the location of the transition depends on the reduced volume and in general approaches L_{cyl} as v is decreased. We therefore expect the curved body to be the only possible equilibrium solution at small reduced volumes for the whole range of $L < L_{cyl}$.

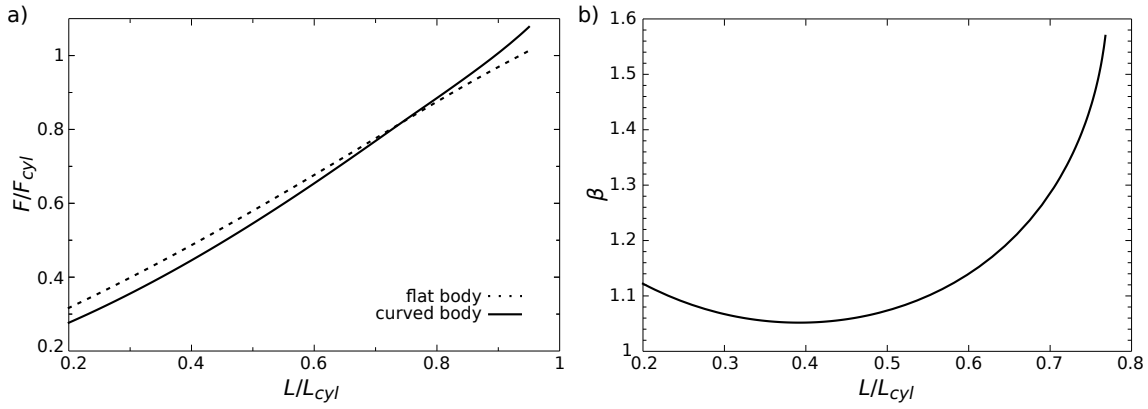

FIG. 6. **Shape of the discoidal body in branch C.** a) The energies of the curved and the flat body structure as functions of the segment length at $v = 0.2$. b) Parameter β representing the degree of curvature as a function of normalised segment length.

COMPARISON BETWEEN ANALYTICAL AND NUMERICAL SOLUTIONS

In order to demonstrate the agreement between our analytical approximations and the general numerical results, we focus on the free energies of the structures. For each specific branch, we use the above mentioned models to calculate the analytical solutions and Surface Evolver package to compute the numerical values. We note that the latter depend on the mesh density (*i.e.* the total number of triangles used for the surface representation) and the lower the density the less accurate the free energy. We therefore compute the energies at three different mesh densities and extrapolate their values to mimic the limit of a smooth surface (*i.e.* infinite mesh density). The errors associated with the numerical solutions are mainly due to the extrapolation process.

Branches A1 and A2

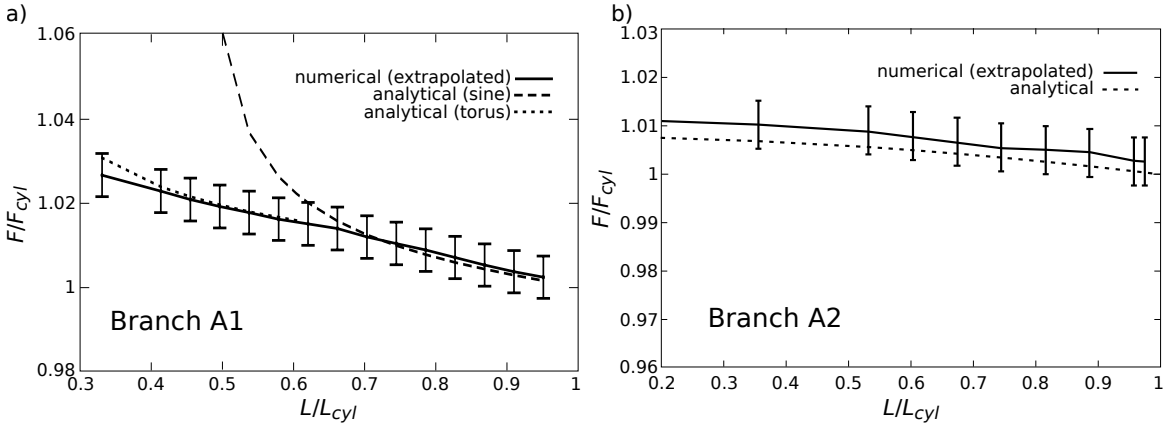

FIG. 7. **Comparison between numerical and analytical solutions in the case of** a) snake-like branch A1 at $v = 0.35$ and b) helical branch A2 at $v = 0.3$. We use both sine and torus model to approximate the behaviour of the branch A1 and we see that even though they eventually diverge, they perform very well in each of their respective regimes. The analytical approximation for the branch A2, on the other hand, demonstrates a great agreement along the whole branch.

Branch B

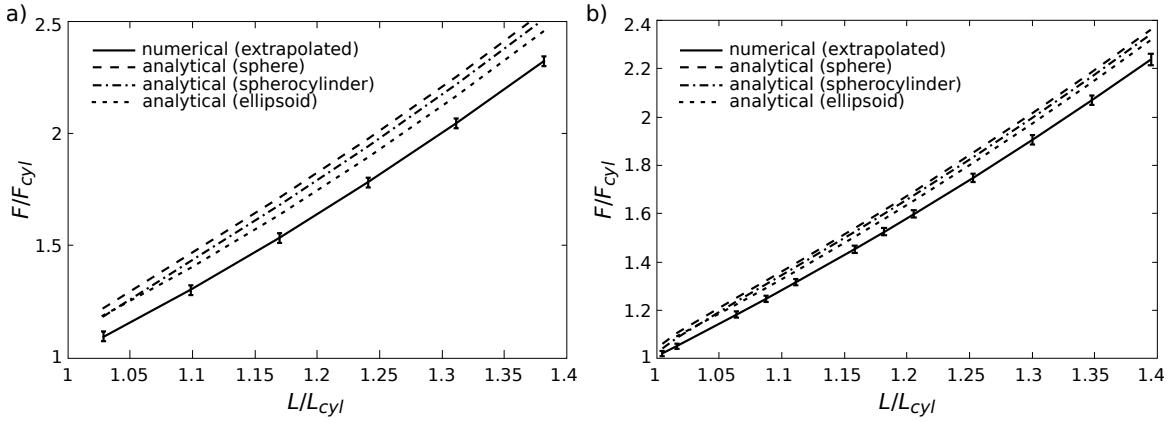

FIG. 8. **Comparison between numerical and analytical solutions for structures in branch B.** The energies are shown at a) $v = 0.3$ and b) $v = 0.2$. We see that in both cases all the analytical solutions cluster together and consistently follow the numerically computed branch. The agreement even furthermore increases as the reduced volume is decreased, thus diminishing the importance of details in modelling the rounded reservoir.

Branch C

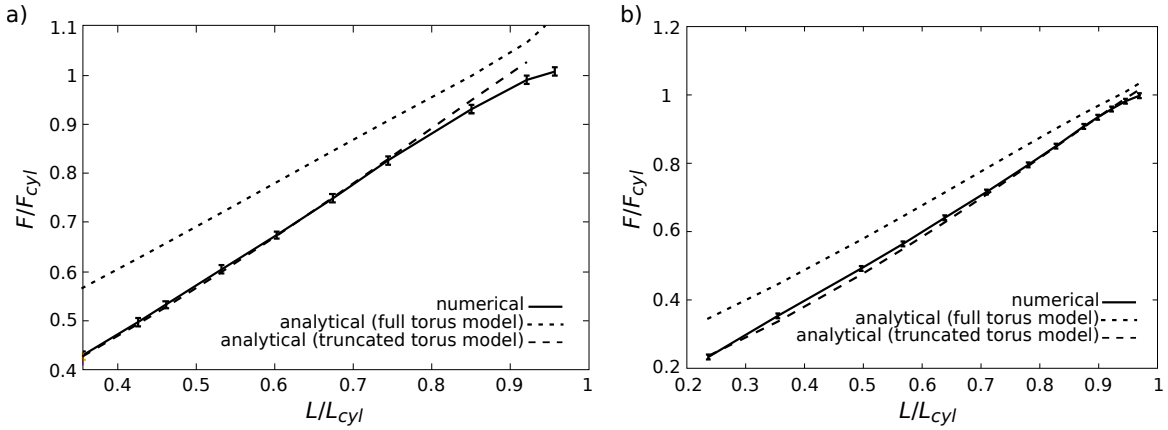

FIG. 9. **Comparison between numerical and analytical solutions for structures in branch C.** The energies are computed at a) $v = 0.3$ and b) $v = 0.2$. Similar to the case of branch B, we observe a good agreement between both types of solutions, with the quality of the analytical approximations increasing as the reduced volume is decreased.